Multimode Jahn-Teller effect in bulk systems: A case of the NV^{0} center in diamond

Jianhua Zhang, Cai-Zhuang Wang, Zizhong Zhu, Qing Huo Liu, and Kai-Ming Ho

Multimode Jahn-Teller Effect in Bulk Systems: A Case of NV^0 Center in Diamond

Jianhua Zhang,[1,2] Cai-Zhuang Wang,[1,*] Zizhong Zhu,[3] Qing Huo Liu,[2,5] Kai-Ming Ho[1,4]

[1]*Ames Laboratory, Iowa State University, Ames IA 50011, USA.*

[2]*Institution of Electromagnetics and Acoustics, and department of Electronic Science of Xiamen University, Xiamen, 361005, China.*

[3]*Collaborative Innovation Center for Optoelectronic Semiconductors and Efficient Devices, Department of Physics, Xiamen University, Xiamen 361005, China.*

[4]*Department of Physics and Astronomy, Iowa State University, Ames, Iowa 50011, United States.*

[5]*Department of Electrical and Computer Engineering, Duke University, Durham, NC 27708 USA.*

Abstract

The multimode Jahn-Teller (JT) effect in a bulk system of neutral nitrogen-vacancy (NV^0) center in diamond is investigated via first-principles density functional theory (DFT) calculations and intrinsic distortion path (IDP) method. The adiabatic potential energy surface (APES) of the electronic ground state of NV^0 center is calculated based on local spin density approximation (LSDA). Our calculations confirm the presence of dynamic Jahn-Teller effect in the ground ^2E state of NV^0 center. Within the harmonic approximation, IDP method provides the reactive path of JT distortion from unstable high symmetry geometry to the stable low symmetry energy minimum geometry and describes the active normal modes participating in the distortion. We find that there are more than one vibrational modes contributing to the distortion and their contributions change along the IDP. Several vibrational modes with large contribution to the JT distortion, especially those modes close to 44 meV, are clearly observed as the phonon sideband in photoluminescence spectra in a serial of experiments, indicating that dynamic Jahn-Teller effect plays an important role on the optical transition of NV^0 center.

I.   Introduction

Nitrogen vacancy (NV) center defect in diamond is extensively studied for a broad range of applications including quantum computation, quantum information process, high sensitivity magnetometry and biosensor due to their unique properties.[1] NV center can exist in two charge states: a neutral (NV^0) state or a negatively charged state (NV$^-$), which can be converted to each other by chemical,[2,3] optical[4] or electrical controlling methods.[5,6] The electronic and optical properties of NV center are directly influenced by atomic vibrations through electron-phonon coupling. The Jahn-Teller (JT) effect in NV center in diamond has attracted a lot of interest in recent years, because electron-phonon interaction and the Jahn-Teller effect are very crucial for understanding the unique properties of the defect. The Jahn-Teller effect has influence on the structure stability of NV center that inducing structure transition from high symmetry C$_{3v}$ geometry to more stable low symmetry C$_{1h}$ geometry for both the ground state of NV^0 center and the excited state of NV$^-$ center. [7,8] The phonon properties of NV center are also affected by the JT effect, especially the symmetry of vibrational modes which have a lower C$_{1h}$ symmetry. [9] The splitting of the double degenerate electronic states under the influence of an e-type distortion in the excited state of NV$^-$ center can also be attributed to the electron-phonon coupling.[10] The JT

effect also plays an important role in the optical properties of NV center. The dynamic JT effect has been used to interpret the temperature dependence of the linewidth of the zero phonon line (ZPL) for the NV$^-$ center[10, 11] and is also responsible for the absence of EPR signal in the ground state of NV^0 center.[12]

The impact of Jahn-Teller effect on the properties of the NV centers has been under investigation from the 1970s-80s.[13-15] Recently, the vibronic properties and JT effect of NV$^-$ center have been continuously investigated by new experiments[11, 16, 17] and *ab initio* calculations.[9, 10, 18, 19] The studies confirm the presence of dynamic JT effect in the exited state of NV$^-$ center.[10, 11] Previous researches showed that the Jahn-Teller effect is observed in the excited state of NV$^-$ center and is invoked to explain the asymmetry between the absorption and photoluminescence (PL) lineshapes.[20] The JT effect has also been used to explain phonon-induced electronic dephasing between the two components of the ^{3}E state.[17] However, unlike NV$^-$ center, there are relatively few reports on the investigation of the JT effect in NV^0. As mention above, dynamic Jahn-Teller effect is regarded as a possible mechanism for the absence of EPR signal in the ground state of NV^0 via broadening the EPR lines to significantly reduce the detection capability.[12] DFT calculations for the vibrational properties and formation free energy of NV centers have been performed to analyze the relative concentration of NV$^-$ and NV^0 defects in diamond. The result demonstrates that the concentration of NV$^-$ becomes greater than that of the NV^0 only when the temperature exceeds 600K.[21] The analysis of the vibronic properties of NV^0 center has also been proceed by other first-principles calculations,[8, 22] and the calculation indicates the exist of JT effect in the ground state of NV^0 center.[8] Despite of these studies, our knowledge about NV^0 center in diamond is still far from complete. Further investigation of the JT effect in NV^0 center can enrich our understanding of the role of JT effect in the process of optical transition and other properties.

When the vibronic coupling is a mechanism responsible for structural distortions and dynamics, there is a cusp in the adiabatic potential energy surface (APES) at the high symmetry (HS) point and the system is unstable. The system will distort to a lower symmetry (LS) energy minimum point by the electron-phonon interaction. In an idea JT case, the JT distortion is represented by the movement of atoms from the HS point along one and only one soft mode of the system which leads the system toward the lower symmetry and lower energy point in APES. However, in the real case there may be many modes coupling to the distortion.[23] To better understanding of multimode problem in Jahn-Teller systems, an intrinsic distortion path (IDP) method has been introduced to provide a detail description of Jahn-Teller distortion and to analyze the role of vibrational modes in the distortion.[24] In the IDP method, the JT distortion is regarded as the superposition of all possible JT active normal modes. Within the harmonic approximation, IDP method provides the reactive path of JT distortion from unstable high symmetry geometry to the stable low symmetry energy minimum geometry and describes the active normal modes participating in the distortion. The method has been widely used in the studies of Jahn-Teller effect in molecular systems.[25-27] In present work, we adopt IDP method to construct a general model for the analysis of the APES of a bulk system of NV^0 center in diamond disposed to the multimode Jahn–Teller effect. We demonstrate that the combination of DFT calculations and IDP method to address the vibronic coupling and contributions successfully describes the dynamic Jahn-Teller effect of the ground state of NV^0 center. To the best of our knowledge, our present

paper is the first time that the scheme is introduced to investigate multimode Jahn-Teller problem in a bulk system. Such an approach will provide a general tool to investigate JT distortion of other similar defects in crystals.

The paper is organized as fellow. In Sec. II we give a brief summary of the computational procedure used in the paper. In Sec. III we analyze APES, IDP, and luminescence lineshape of NV^0 center in detail. In Sec. IV we show the conclusion of the paper.

II. Methods

2.1. Density functional calculations of the structure and vibrational modes of NV^0 center

Previous *ab initio* calculations have shown that DFT works well in the study of electronic and vibronic (phonon) properties of NV^0 center.[8, 21] In our present work, density functional theory calculations are carried out using the plane wave basis code as implemented in the Vienna *ab initio* Simulation Package (VASP) with the local spin density approximation (LSDA).[28] The Γ point for k-point sampling and a plane-wave basis set with an energy-cutoff of 420 eV are used in our calculations. In the geometry optimization calculations, a 215-atom cubic supercell (3×3×3) with the box length of $3a_0 = 10.605$ Å is used, where a_0 is the optimized equilibrium lattice constant of the diamond structure. All internal atomic positions are relaxed in a constant volume until the forces are below 10^{-3} eV/Å on every atom.

The atomic structure of the NV^0 center in its electronic ground state has been optimized before the calculation for the vibration modes are performed. The vibrational modes for the ground state of the NV^0 center are performed using finite displacement method.[29] The dynamics matrix of the supercell containing a NV^0 center defect is obtained from a set of force calculations, in which atoms in the supercell is selected one-by-one to displace with a small displacement (0.02 Å) from its equilibrium position. Diagonalization of the 645×645 dynamics matrix provides the frequencies and eigenvectors of the 642 vibrational modes and three translational modes. The degree of the mode localization can be quantified by its inverse participation ratio (IPR), defined as[9, 30]

$$IPR_k = \sum_{i=1}^{N} (\boldsymbol{u_i} . \boldsymbol{u_i})^2 \left(\sum_{i=1}^{N} \boldsymbol{u_i} \cdot \boldsymbol{u_i} \right)^{-2} \tag{1}$$

where $\boldsymbol{u_i}$ is the normalized three-dimensional atomic displacements of the atom i in the corresponding eigenvector of vibrational mode k and N is the number of atoms in the system. It is obvious that IPR_k reflects a typical number of atoms participating effectively in the vibrational mode k. For completely delocalized phonons $IPR_k \sim 1/N$ is almost zero for macroscopic systems, while for a completely localized mode IPR_k is finite independently of the system size.

2.2 DFT calculations of JT properties and potential energy surface of NV^0 center

The NV^0 center has ^{2}E electronic ground state in the high symmetry atomic configuration. This atomic configuration is not a stationary point on potential energy surface, and there is coupling between the E electronic states with the non-totally symmetric e vibrations. Therefore, our procedure for calculating the JT parameters consists of the following steps:[31] (i) a geometry optimization of NV^0 center in a high C$_{3v}$ symmetry with an occupation of 0.5 on both e orbitals, $(e_x)^{0.5} (e_y)^{0.5}$. (ii) Energy calculation using the high symmetry geometry (G$_{HS}$) obtained by step (i) and with the electronic configuration as that in the lower symmetry structure. This is achieved by doing calculation with an integer occupation on one of the doubly degenerate orbitals, e.g., $(e_x)^1$ $(e_y)^0$. (iii) A complete geometry optimization on the lower symmetry structure, with the same electron occupancy in step (ii). This results in two different geometries with low C$_{1h}$ symmetry, i.e., a geometry at the energy minimum (G$_M$) and a geometry at the saddle point (G$_S$), respectively. A vector $\vec{R}_{JT}$ in the APES defines the straight path (also called Direct Path) from the G$_{HS}$ to the G$_M$. Similarly, $\vec{R}_S$ defines the straight path (Direct Path) from the G$_S$ to the G$_M$. E$_{JT}$ is the difference between the energies of the G$_{HS}$ in the steps (ii) and the G$_M$ in step (iii). The energy difference between G$_S$ and G$_M$ is the warping barrier, δ. The energies of the lower branch of the APES are obtained along the direct path $\vec{R}_{JT}$ and $\vec{R}_S$ with the orbital occupancy $(e_x)^1 (e_y)^0$. The energies of the upper branch of APES are obtained by promoting one electron from the e_x to e_y with the same geometries of the lower branch.

2.3 Intrinsic Distortion Path (IDP)

The reaction path starting from high symmetry geometry G$_{HS}$ to low symmetry minimum G$_M$ is defined as 'intrinsic distortion path (IDP)'.[24] In the IDP method, each point X in the APES can be represented as a 3N-dimentional vector $\vec{R}_X$, and the energy minimum point M is taken as the origin point ($\vec{R}(G_M) = 0$). Within harmonic approximation, the distortion $\vec{R}_X$ can be written as a linear combination of all (N$_{a1}$) totally symmetric normal modes in the G$_M$,

$$\vec{R}_X = \sum_{k=1}^{N_{a1}} w_{Xk}\vec{Q}_k, \tag{2}$$

where $\vec{Q}_k$ are mass-weighted totally symmetric normal coordinates, which are the eigenvector of the corresponding vibrational mode in the G$_M$. w_{Xk} are weighing factors representing the contribution of different mode to the distortion. The energy difference (E_X) between the point X and G$_M$ can be obtained from a sum of the energy contributions of all totally normal modes in the G$_M$:

$$E_X = \sum_{k=1}^{N_{a1}} E_k = \frac{1}{2}\sum_{k=1}^{N_{a1}} w_{Xk}^2 \vec{Q}_k^2 \nu_k, \tag{3}$$

where w_{Xk} is obtained from equation (2), ν_k and $\vec{Q}_k$ are frequency and eigenvector of the corresponding vibrational mode in the G$_M$, which are obtained from the DFT calculation. When the point X is corresponding to the high symmetrical geometry ($\vec{R}_X = \vec{R}_{JT}$), we then obtain JT energy: E$_{JT}$. The APES constructed by the IDP method is a simplified quadratic energy surface, which can be deviated from the APES obtained directly from DFT calculations which include also the effects of anharmonicity. However, it is found that most of the results obtained from IDP method with harmonic approximation are in a good agreement with DFT calculations.[25] The driving forces on the unstable point X on the APES can directly obtained from the derivation of

energy over Cartesian coordinates. The total force can be expressed as a vector sum of the individual forces:

$$\vec{F}_{Xtot} = \sum_{k=1}^{N_{a1}} \vec{F}_{Xk} = \frac{1}{2}\sum_{k=1}^{N_{a1}} w_{Xk} v_k M^{1/2}\vec{Q}_k, \tag{4}$$

where M is a diagonal 3N×3N matrix with atomic masses in triplicates as elements (m_1, m_2, m_3, m_4, ..., m_n).[24] The force will drive the system from the cusp to the minimum energy point step-by-step on the APES in a fast energy minimization manner. In this process, the path that the system covered is IDP, which is in general different from the Direct Path mentioned above. The energies and forces of the points along the IDP can be recorded by equations (2-4). The contribution of all the totally-symmetric modes to the distortion and their changes along the IDP can also be distinguished. Details about this method have been represented in the previous work. [24, 31]

2.4 Luminescence lineshape and Huang-Rhys (HR) factor

We adopt the method introduced by Alkauskas et. al. to calculate the luminescence lineshape and HR factor for the neutral NV center.[19] The method has been successfully used in the study of the negatively charged NV center. According this method, the normalized luminescence intensity is expressed as

$$L(\hbar\omega) = C\omega^3 A(\hbar\omega), \tag{5}$$

where C is a normalization constant:

$$C^{-1} = \int \omega^3 A(\hbar\omega)\, d(\hbar\omega), \tag{6}$$

and $A(\hbar\omega)$ is optical spectral function which is defined as the Fourier transform of a generating function $G(t)$:[32, 33]

$$A(E_{ZPL} - \hbar\omega) = \frac{1}{2\pi}\int_0^\infty G(t)e^{iwt-\gamma|t|}d(t), \tag{7}$$

where the parameter γ represents the broadening of the ZPL and is chosen to reproduce the experimental width of the ZPL.

The generating function $G(t)$ is defined as

$$G(t) = e^{S(t)-S(0)}, \tag{8}$$

where

$$S(t) = \int_0^\infty S(\hbar\omega)e^{-iwt}d(\hbar\omega). \tag{9}$$

$S(\hbar\omega)$ is the spectral function of electron-phonon coupling which is defined as

$$S(\hbar\omega) = \sum_k S_k\delta(\hbar\omega - \hbar\omega_k), \tag{10}$$

where ω_k is the frequency of the vibrational modes k, and S_k is the (partial) HR factor for the mode k. It is calculated as:[34]

$$S_k = \omega_k q_k^2/(2\hbar), \tag{11}$$

with

$$q_k = \sum_{\alpha i} m_\alpha^{1/2}\big(R_{e;\alpha i} - R_{g;\alpha i}\big)\Delta r_{k;\alpha i}, \tag{12}$$

where α labels atoms, $i = \{x, y, z\}$, m_α is the mass of atom α, $R_{\{e,g\};\alpha i}$ is the equilibrium position in the initial (excited) and the final (ground) state, and $\Delta r_{k;\alpha i}$ is a normalized vector that describes the displacement of the atom α along the direction i in the phonon mode k.

The total HR factor for a given optical transition is obtained by

$$S \equiv S(t=0) = \int_0^\infty S(\hbar\omega)d(\hbar\omega) = \sum_k S_k. \tag{13}$$

More details of the calculations can be found in the previous work.[19]

Taken the atomic positions of the energy minimum point M in the APES as reference, the position deviation of the point X from the energy minimum point M in the APES can be described by 3N equations:

$$R_{X;\alpha i} = R_{g(X);\alpha i} - R_{g(M);\alpha i}, \tag{14}$$

where α and i have the same meaning in the Eq. (12), $R_{g(X);\alpha i}$ and $R_{g(M);\alpha i}$ is the atomic position in the point X and the low symmetry minimum G_M in the APES of the neutral NV center in the ground state. In special, when $\vec{R}_X = \vec{R}_{JT}$, we have:

$$R_{JT;\alpha i} = R_{g(HS);\alpha i} - R_{g(M);\alpha i}, \tag{15}$$

where $R_{g(HS);\alpha i}$ is the atomic position in the high symmetry geometry G_{HS}. From Eq. (2), we can obtain 3N equations:

$$\left(R_{g(HS);\alpha i} - R_{g(M);\alpha i}\right) = \sum_{k=1}^{N_{a1}} w_k \Delta r_{k;\alpha i}, \tag{16}$$

where w_k are weighing factors representing the contribution of different mode to the distortion $\vec{R}_{JT}$ and $\Delta r_{k;\alpha i}$ has the same definition in the Eq. (12). In Eq. (12), the equilibrium atomic position in the final (ground) state is exactly the one in the energy minimum geometry: $R_{g;\alpha i} = R_{g(M);\alpha i}$. In general, the equilibrium atomic position $(R_{e;\alpha i})$ in the excited state may not equal to the one $(R_{g(HS);\alpha i})$ in the high symmetry geometry G_{HS} in the ground state. However, these two geometries have the same (C_{3V}) symmetry and their distortions from the low symmetry minimum G_M in the ground state have positive correlation: $\left(R_{g(HS);\alpha i} - R_{g(M);\alpha i}\right) \sim \left(R_{e;\alpha i} - R_{g;\alpha i}\right)$ found in our calculations. Thus, from equation (11), (12) and (16), we can obtain:

$$q_k = \sum_{\alpha i} m_\alpha^{1/2}\left(R_{e;\alpha i} - R_{g;\alpha i}\right)\Delta r_{k;\alpha i} \sim \sum_{\alpha i} m_\alpha^{1/2} \sum_{k=1}^{N_{a1}} w_k \Delta r_{k;\alpha i}^2, \tag{17}$$

and

$$S_k = \omega_k q_k^2/(2\hbar) \sim \omega_k\left[\sum_{\alpha i} m_\alpha^{1/2} \sum_{k=1}^{N_{a1}} w_k \Delta r_{k;\alpha i}^2\right]^2/(2\hbar). \tag{18}$$

Therefore, there is a strong positive correlation between partial Huang-Rhys factors S_k and the weighting factor w_k, which represents the contribution of different mode to the JT distortion.

III. Results and Discussion

3.1 Geometry optimization and JT distortion energy

The neutral nitrogen-vacancy color center consists of a substitutional nitrogen atom (N) and an adjacent vacancy (V) in the diamond lattice. It has trigonal C_{3v} symmetry in the ^2E ground state. The defect state of NV^0 center can be described by the five-electron model:[8] two fully symmetric singlet a_1 states $(u\bar{u}v\bar{v})$ and one doubly degenerate e state $(e_x\bar{e}_x e_y\bar{e}_y)$, with an occupation of five electrons $u^2v^2e^1$ in the ^2E ground state. Here u denotes a spin up state while $\bar{u}$ denotes a spin down state. The coupling between the twofold degenerate electronic E states and the twofold degenerate e vibrations will result in an $E \otimes e$ JT problem in the ground state of NV^0 center.

The occupation of defect levels in the band gap of diamond and the optimized structure around vacancy obtained from our calculation are shown in Fig. 1. Following the computational step (i) mentioned above, the geometry optimization is initialized from the high symmetry C_{3v} geometry

with half occupied two degenerate e levels: $(e_x)^{0.5} (e_y)^{0.5}$, and the C_{3v} symmetry is found to be kept after optimization. Then the system energy is calculated when one of two degenerate levels is occupied $((e_x)^1 (e_y)^0)$ as mentioned in the step (ii) and the results are shown in the middle panel of Fig. 1. After geometry optimization, the bond length of three carbon atoms adjacent to the vacancy are equivalent (2.635 Å), forming an equilateral triangle. And the bond lengths of the nitrogen atom with these carbon atoms are also equivalent (2.715 Å).

Following the step (iii) described in the method section, two geometries with C_{1h} symmetry are obtained after optimization: the carbon atoms adjacent to the vacancy forms acute (Fig.1, left panel) or obtuse (Fig.1, right panel) isosceles triangles. One of them is at the energy minimum (denoted as M) and the other is a saddle point (denoted as S) on the APES. The corresponding Jahn-Teller distortion energies E_{JT}^M and E_{JT}^S are 73.2 meV and 63.2 meV, respectively. The energy difference between the C_{3v} and C_{1h} geometries of the neutral NV center in diamond at ground state are also obtained by first-principles calculations with LDA potential.[8] The energy barrier (δ) between the two low symmetry geometries (G_M and G_S) is 10 meV. The distortion distances from the high symmetry geometry to the two low symmetry geometries R_M and R_S are 0.101 Å and 0.127 Å, respectively. The results can also be seen in Table I.

3.2 APES: Coupling of electronic E states and the double degenerate e vibration modes and the dynamic Jahn-Teller effect

Since the ground state of NV^0 center in diamond with the C_{3v} symmetry belongs to an $E \otimes e$ JT system in which the doubly degenerate electronic E states are coupled with the doubly degenerate e vibrational states, the distortion coordinate is e ($E \otimes E = A_1 + [A_2] + E$) and the decent of symmetry goes to C_{1h} according to group theory. In this case, the irreducible representation of the active modes becomes totally symmetric.

For the ground state of neutral vacancy center in diamond, the degenerate electronic E states ($\psi_\varepsilon, \psi_\theta$) can be perturbed by the vibration e modes (Q_ε, Q_θ), besides being perturbed by totally symmetric atomic movements. Considering the electron-phonon interaction, according to the Jahn-Teller theory, the adiabatic potential energy surface can be written in a polar coordinate form ($Q_\varepsilon = \rho \sin\varphi$, $Q_\theta = \rho \cos\varphi$),[35]

$$\varepsilon_\pm(\rho, \varphi) = V_{2a}\rho^2 + V_{3a}\rho^3 cos3\varphi \ \pm \rho[(V_{1e}^2 - 2V_{1e}V_{2e}\rho cos3\varphi) + (2V_{1e}V_{3e} + V_{2e}^2)\rho^2 -$$
$$(2V_{2e}V_{3e}^3 cos(3\varphi))\rho^3 + V_{3e}\rho^4]^{1/2}, \tag{19}$$

where V_{2a} (V_{3a}) is an elastic (cubic) force constant, and V_{ie} ($i = 1,2,3$) are linear, quadratic, and cubic coupling parameters. Neglecting the parameter V_{3e}, which may not have significant contribution to the APES $\varepsilon_\pm$,[35] we expand the equation (19) in the third order in ρ:

$$\varepsilon_\pm(\rho, \varphi) = V_{2a}\rho^2 + V_{3a}\rho^3 cos3\varphi \ \pm \rho[(V_{1e}^2 - 2V_{1e}V_{2e}\rho cos3\varphi) + V_{2e}^2\rho^2]^{1/2}. \tag{20}$$

If one includes only the linear JT coupling, the APES will show radial symmetry, resembling the well-known Mexican hat shape. In our study, two methods are introduced to fit the *ab initio* data of the APES based on the analytical expression of Eq. (20) and up to third order in ρ. One is to fit both the upper and lower branches of the APES (ε_+ and ε_-) simultaneously, and the other is to fit the two curves, $(\varepsilon_+ + \varepsilon_-)/2$ and $(\varepsilon_+ - \varepsilon_-)/2$, separately.[35] The fitting parameters from both fitting methods are shown in Table II. The corresponding results are compared with the *ab initio* data as shown in Fig. 2. The frequency of the effective coupling vibrational mode can be

estimated using the elastic constant V_{2a}.[10] The energy ($\hbar\omega$) of the vibrational mode is about 62.5 meV obtained by both fitting methods. This energy is close to the energy (about 70 meV) of the effective vibrational mode of NV^0 center in the ground state.[13, 15] Unlike the case in the negatively charged NV center,[10] which has a weak coupling constant $\lambda = E_{JT}/\hbar\omega < 1$, in the present ab initio calculations, the coupling constant of NV^0 center are strong due to that $\lambda = E_{JT}/\hbar\omega = 1.17 > 1$, but not very strong. This is consistent with the statements in Ref.[13] that the consequence of the JT effects at deep centers in diamond is different for ground-state and excited states. All the known orbitally degenerate ground states undergo significant relaxations ($\lambda > 1$), while all the degenerate excited states have small or negligible relaxations ($\lambda < 1$). However, it is worth noting that Davies used a bigger value of λ ($= 2$) in his discussion of NV^0 center by assuming that the JT relaxation is a significant contributor to the bandshape.[13]

Furthermore, adiabatic potential energy surface and contour plot of the lower sheet of ^2E state are shown in Fig. 3. Three equivalent minima (at $\theta = 0, 2\pi/3, 4\pi/3$) separated by three saddle points are found in the lower sheet of the APES. From first-principles calculations, the barrier height δ between the minima is 10 meV, which is close to the experiment result 28 meV.[15] The smaller energy barriers we got may be due to LDA tends to underestimate the barrier energy. In the case that the barrier height δ ($= 10\ meV$) is smaller than the phonon energy $\hbar\omega$ ($= 62.5\ meV$), the vibration can help atoms to hop between the three equivalent C_{1h} configurations in the Q_ε, Q_θ space much more easily and the system exhibits an effective C_{3v} symmetry, as predicted by dynamic Jahn-Teller theory.

According to the JT parameters obtained in Table II, we can also perform the calculations of effective vibronic energies via diagonalizing the vibronic Hamiltonian:

$$H = H_0 - \hbar^2/2M\left(\partial^2/\partial Q_\theta^2 + \partial^2/\partial Q_\varepsilon^2\right) + U_\theta\left[V_{1e}Q_\theta + V_{2e}\left(Q_\varepsilon^2 - Q_\theta^2\right)\right] + U_\varepsilon[V_{1e}Q_\varepsilon + V_{2e}(2Q_\varepsilon Q_\theta)] + I\left[V_{2a}\left(Q_\theta^2 + Q_\varepsilon^2\right) + V_{3a}\left(Q_\theta^3 - 3Q_\theta Q_\varepsilon^2\right)\right] \tag{21}$$

where H_0 is the Hamiltonian of degenerate electronic state at $Q_\varepsilon = Q_\theta = 0$, and U_ε, U_θ and I are 2×2 matrix: $U_\varepsilon = \begin{pmatrix} 1 & 0 \\ 0 & -1 \end{pmatrix}$, $U_\theta = \begin{pmatrix} 0 & 1 \\ 1 & 0 \end{pmatrix}$, and $I = \begin{pmatrix} 1 & 0 \\ 0 & 1 \end{pmatrix}$. The vibronic Hamiltonian can be diagonalized in a symmetry adapted vibronic basis constructed from the direct product of the electronic wave-function $\phi_j(\vec{r})(j = 1, 2)$ and the states of the harmonic oscillators $\chi_{n_\varepsilon}(Q_\varepsilon)$ and $\chi_{n_\theta}(Q_\theta)$:

$$\psi_{j,n_\varepsilon,n_\theta} = \phi_j(\vec{r})\chi_{n_\varepsilon}(Q_\varepsilon)\chi_{n_\theta}(Q_\theta). \tag{22}$$

The results for the lowest few vibronic states are shown in Table III. The first excited nondegenerate state (A_2) above the vibronic ground E state obtained from our calculation is a little larger ($3\Gamma = 21.4$ meV (or 23.8 meV)) than that ($3\Gamma = 13.6\ meV$ ($110\ cm^{-1}$)) mentioned in Ref. 13. The splitting 3Γ between the E-type vibronic ground state and the A-type first excited state is the so-called tunneling splitting.[23] Similar to the negatively charged NV, the energy barrier ($\delta = 10\ meV$) between the APES minima from the present ab initio calculation is rather small that the concept of occasional tunneling between localized vibration states is also not valid for the neutral NV center. However, we can still use the energy splitting 3Γ as a measure of the degree of the localization (or delocalization) of the vibrational states.[18] For the neutral NV center, the barrier to tunneling splitting ratio, $\delta/3\Gamma$ is 0.47 (or 0.42), indicating that the system is also a dynamic Jahn-Teller system. Our calculations also show that there is another A_1 state at 38.5 meV (or 30.8 meV) above the E vibronic ground state. This is consistent with the results in Ref. 13, in which Davies predicted an A_1 state to lie at an energy

8

$\Delta + 3\Gamma = 45.9 \pm 24.8$ meV (370 ± 200 cm^{-1}) above the E vibronic ground state and he also obtained a value $35.3 \left(^{+18.6}_{-6.2}\right)$ meV ($285 \left(^{+150}_{-50}\right)$ cm^{-1}) of the A_1 state from the fit to their stress data to support his prediction.

3.3 Intrinsic Distortion Path (IDP)

The energy variation of the defect along IDP is showed in Fig. 4(a). The JT energy obtained by the IDP method is 60.9 meV, which is smaller than the one (73.2 meV) obtained from DFT method due to lack of the anharmonic effect in IDP. The decrease of energy along IDP is faster than that along the direct path in the early time of distortion process. Then the energy falls gradually to zero, in the meantime the system relaxes to the C_{1h} minimum point. Overall, the deviation of the reactive path from the two paths is small. As mentioned above, the number of the vibrational modes of system is 3N-3 (= 642) in our calculations. But not all these modes have contribution to the distortion form the G_{HS} to the G_M. In our calculations, we find that 338 totally symmetry modes have contribution to the JT distortion. Among these modes, we chose the most important 14 normal modes shown in Table IV. These 14 modes have 86.8% contribution to the JT distortion and 63.4% contribution to the JT energy (Table IV). Most of the modes with large contribution to the JT distortion are soft modes. It is noteworthy that not all these modes are quasilocalized modes, some of them have small IPR as shown in Table IV. In addition, we also find that several modes with large frequency not shown in the Table IV (e.g., the hardest modes: 167.2 meV) also have large contribution (2.7%) to the JT distortion energy.

The contributions of the most important totally symmetric modes to the JT distortion along the IDP are illustrated in Fig. 4(b). At start point (G_{HS}), one quasilocalized mode with an energy of 52.9 meV has the largest contribution to the distortion (39.1%). The contribution decreases along the IDP, and finally gets to a value less than 20% when it is close to the LS geometry G_M. In the contrast, the contributions of other three normal modes around 45.0 meV (44.2, 45.6, and 46.7 meV) increase along the IDP and get their maximum contributions at the G_M, especially for the mode of 44.2 meV, whose contribution stands over 50%. It indicates that these modes dominate the relaxation of the geometry near the G_M. The contributions of the other modes (e.g., 65.1 meV etc.) decrease along the IDP gradually and fade out when approaching G_M.

In order to see the details of the coupling vibrational modes, the motions of the atoms in the normal modes are extracted from the corresponding eigenvectors of the vibration modes. Here we represent atomic vibration patterns of the two important modes (44.2 and 52.9 meV) with the largest contribution to the distortion in Fig. 5. The atoms around the vacancy have large degree of displacement and the modes favorite the bond-bending patterns.

The driving forces along the IDP are shown in Fig. 6. The modes with the largest forces could generally be divided into two categories: the hard modes and the soft ones. For the seven hardest modes (167.2, 161.6, 164.0 158.7, 166.4 164.8 and 159.5 meV) in the ground state of NV^0 center, the forces along the IDP decrease rapidly to nearly zero once R_X/R_{JT} reaches 0.6. It is the primary cause of the energy reduction in the early stage of the distortion. By contrast, the forces from soft modes (52.9, 83.1, 64.1, 74.2, and 44.2 meV) reduce slowly along the IDP.

The important coupling modes with energies of 44.2, 45.6 and 46.7 meV stay in the range of the effective phonon energy (37.2 meV~104.2 meV) and are close to a sideband of 45 meV

illustrated by Davies.[13] Moreover it is also in excellent agreement with the observations in the PL-spectra of NV^0 diamond: one clear sideband at about 44 meV is found both in the Fig. 1(a) of reference 36 and Fig. 2(a) of reference 37. Besides, photoluminescence studies also shows that the vibrations of NV^0 involve one phonon with energy of 42 meV.[38] In addition, the quasilocalized vibrational modes (74.2 and 72.6 meV) with small IPR, which also have large contribution to the JT distortion, are in a good agreement with the effective mode about 70 meV inferred by experiment[13, 15] and the activated mode about 75 meV evaluated by quantum chemical calculation.[22] This implies that the vibration modes coupled to JT distortion could play an important role in optical properties of NV^0 center if we assume that the Jahn-Teller effect has a significant contribution to the bandshape.

We also performed the calculations to study the intrinsic distortion path with a larger supercell (4×4×4) to see whether the main results we obtained from the (3×3×3) supercell are reliable. The JT energy of the (4×4×4) 511-atom supercell is obtained in the same way as in the 215-atom supercell calculation. The vibrational modes of the 511-atom supercell are calculated using the method proposed in the Ref. 19. The comparison of the IDP between the 215-atom and 511-atom supercells is shown in Fig. 7. For both supercells, their energy changes from the G_{HS} to the G_M along the IDP are very close to each other, especially when the geometries are close to the G_M (Fig. 7a). The deviation between them increases with the value of R_X/R_{JT} and gets its maximum when $R_X/R_{JT} = 1$. The JT energy of 511-atom supercell obtained from IDP method is 67.8 meV, which is a little bigger than the one (60.9 meV) from 215-atom supercell but is very close to the one (69.9 meV) from fully ab initio calculation for the 511-atom supercell. Since the number of vibrational modes in the 215-atom and 511-atom supercells is not the same, it is convenient to compare the contributions of the vibrational modes to the JT distortion from both supercells by looking at the energy-dependence spectra of the contribution. Using a Gaussian smoothing scheme, the spectra of the contributions of vibrational modes to the JT distortion in both supercells are compared in Fig. 7b. Comparison shows that the spectra of the two supercells are in good agreement. Since the JT energy, IDP, and the contributions of vibrational modes from the 215-atom supercell and 511-atom supercell calculations are very similar, we believe that the 215-atom supercell is suitable for the investigation of the multimode Jahn-Teller effect in the ground state of the neutral NV center.

3.4 HR factor and luminescence lineshape

To further examine the role of the JT relaxation on the optical transition, we investigate the contribution of the JT active modes to the vibronic spectra by calculating the HR factor and luminescence spectrum. The HR factor is used to characterize vibrational structure of the luminescence band. The total HR factor S defined in equation (13) describes the total number of phonons emitted during the optical transition. The calculated total HR factor is $S = 2.79$, a little smaller than the expected value ($S = 3$) from experiment.[13] The smaller value of HR factor could be attributable to DFT method and the psedopotential used in our calculations. Similar results have also been reported for DFT calculation at PBE level of negatively charged NV center.[19] The partial HR factor S_k represents the average number of phonons of type k emitted during the optical transition.[39] So S_k can be treated as an important parameter describing the relationship between the vibrational mode k and the sideband in the luminescence spectra. The vibrational

modes with the two largest values of S_k are at 44.2 meV ($S_k = 0.778$) and 52.9 meV ($S_k = 0.378$) respectively, which are the modes having large contribution to the JT distortion.

The calculated luminescence lineshape and its comparison with the experimental results are shown in Fig. 8. The lineshape from the calculation qualitatively agrees with the experiments,[13, 36-38] especially for the main phonon replicas at about 44-46 meV and 89-90 meV, though there are quantitative differences. Similar quantitative differences between the calculations at PBE levels and the experiment can also be found in the investigation of the negatively charged NV center.[19] The active phonon mode at 44.2 meV in the JT distortion, which is found to have the largest contribution to HR factor S, produces an obvious phonon sideband in the luminescence lineshape. Because of this, we suggest that dynamic Jahn-Teller effect could play an important role on the optical transition of NV^0 center.

IV. Conclusion

We investigated the multimode Jahn-Teller effect of NV^0 center in diamond using both DFT and IDP methods. The methods open a road to analysing the multimode JT distortion of bulk system and provide the description of JT properties with reliable accuracy. We obtain the energies on the APES from DFT calculations, and fit the data with an analytical expression of APES to get the vibronic coupling parameters. The calculation shows that the quadratic JT coupling induces the bottom of the APES to be warped with alternating three global minima separated by three saddle points. Free rotation between the three minima are expected to be present because the energy of coupling virational mode is bigger than the warping barrier ($\hbar\omega > \delta$). From the analysis of APES, we confirm that the ground state of NV^0 center is a dynamic JT system, which is consist with the observation by Davies in the 1970s-80s[13-15] and recent *ab initio* results from Gali et. al.[8]

By extending the IDP method from molecular system to a bulk crystal system (diamond) with a defects (NV^0 center), we demonstrated advantages of the IDP method in the investigation of multimode JT distortion of defects in crystals. One of them is selecting a true LS energy minimum on the APES as reference point. The JT distortion is given as a superposition of all-totally symmetric normal modes of the reference point. As we know, there is no practical method to calculate the frequency of HS unstable point.[10] One can also use finite displacement method to calculate the phonon modes of HS unstable point, but that will contain some negative modes, which may be not suitable (or convenient) for the analysis of JT effect. The second is that within the harmonic approximation, IDP method treats the JT distortion in a simple form. This will help one to analyze the JT effect more efficiently, and bring more convenience for the calculation of reactive path of JT distortion. However, for the same reason, IDP method has disadvantage that it does not include the anharmonicity of electron-phonon coupling, which should be considered in the further studies. For the multimode Jahn-Teller effect, how many normal modes have contribution to the distortion; how to distinguish them and how do they change along the IDP? These questions are very important for understanding the mechanism of JT distortion. IDP method provides the related active modes, their contribution to the distortion, and the change of the contribution along the IDP. Therefore, another advantage of IDP method is that it provides more details of electron-phonon coupling in the JT systems.

We specifically pick up the neutral NV center in diamond as an example of bulk system for the use of IDP method, due to that the NV center in diamond is very important and extensively

studied recently. The results of IDP method are consistent with the DFT calculations. We find several key modes coupling to the JT distortion, some of them can be directly observed in photoluminescence band in several different experiments. It is important to note that most of the normal modes with large contribution to the distortion of NV^0 center are soft modes, which are not all quasilocalized vibrational modes. However, through analyzing the change of forces along IDP from the G_{HS} to the G_M, the hard modes (with large frequencies) are also found to play an important role at early stage, causing the energy fell quickly in the beginning, while the soft modes with large contribution to the distortion dominate the relaxation part of the reactive path. This phenomenon is similar to that of the JT systems in molecules.

In summary, we have demonstrated that the combination of DFT and IDP methods can be considered as powerful tools for the investigation of adiabatic potential energy surfaces of JT active systems and for better understanding the multimode Jahn-Teller effect of defects in crystals.

Reference

[1] M. W. Doherty, N. B. Manson, P. Delaney, F. Jelezko, J. Wrachtrup, and L. C. L. Hollenberg, Phys. Rep.-Rev. Sec. Phys. Lett. **528**, 1 (2013).

[2] K. M. C. Fu, C. Santori, P. E. Barclay, and R. G. Beausoleil, Applied Physics Letters **96**, 121907 (2010).

[3] M. V. Hauf, B. Grotz, B. Naydenov, M. Dankerl, S. Pezzagna, J. Meijer, F. Jelezko, J. Wrachtrup, M. Stutzmann, F. Reinhard, and J. A. Garrido, Phys. Rev. B **83**, 081304 (2011).

[4] X. D. Chen, C. L. Zou, F. W. Sun, and G. C. Guo, Applied Physics Letters **103**, 013112 (2013).

[5] B. Grotz, M. V. Hauf, M. Dankerl, B. Naydenov, S. Pezzagna, J. Meijer, F. Jelezko, J. Wrachtrup, M. Stutzmann, F. Reinhard, and J. A. Garrido, Nat. Commun. 3, **729** (2012).

[6] J. C. A. Prentice, B. Monserrat, and R. J. Needs, Phys. Rev. B **95**, 014108 (2017).

[7] A. Gali, M. Fyta, and E. Kaxiras, Phys. Rev. B **77**, 155206 (2008).

[8] A. Gali, Phys. Rev. B **79**, 235210 (2009).

[9] J. Zhang, C.-Z. Wang, Z. Z. Zhu, and V. V. Dobrovitski, Phys. Rev. B **84**, 035211 (2011).

10   T. A. Abtew, Y. Y. Sun, B.-C. Shih, P. Dev, S. B. Zhang, and P. Zhang, Phys. Rev. Lett. **107**, 146403 (2011).

11   K.-M. C. Fu, C. Santori, P. E. Barclay, L. J. Rogers, N. B. Manson, and R. G. Beausoleil, Phys. Rev. Lett. **103**, 256404 (2009).

12   S. Felton, A. M. Edmonds, M. E. Newton, P. M. Martineau, D. Fisher, and D. J. Twitchen, Phys. Rev. B **77**, 081201 (2008).

13   G. Davies, Journal of Physics C: Solid State Physics **12**, 2551 (1979).

14   G. Davies and C. Foy, Journal of Physics C: Solid State Physics **13**, 2203 (1980).

15   G. Davies, Reports on Progress in Physics **44**, 787 (1981).

16   V. M. Huxter, T. A. A. Oliver, D. Budker, and G. R. Fleming, in *Xviiith International Conference on Ultrafast Phenomena*, edited by M. Chergui, A. Taylor, S. Cundiff, R. DeVivieRiedle and K. Yamagouchi (E D P Sciences, Cedex A, 2013), Vol. 41.

17   R. Ulbricht, S. Dong, I. Y. Chang, B. M. K. Mariserla, K. M. Dani, K. Hyeon-Deuk, and Z. H. Loh, Nat. Commun. **7**, 6 (2016).

18   A. Gali, T. Simon, and J. E. Lowther, New J. Phys. **13**, 025016 (2011).

19   A. Alkauskas, B. B. Buckley, D. D. Awschalom, and C. G. Van de Walle, New J. Phys. **16**, 23 (2014).

20   M. W. Doherty, N. B. Manson, P. Delaney, F. Jelezko, J. Wrachtrup, and L. C. L. Hollenberg, Physics Reports **528**, 1 (2013).

21   B. T. Webber, M. C. Per, D. W. Drumm, L. C. L. Hollenberg, and S. P. Russo, Phys. Rev. B **85**, 014102 (2012).

22   A. S. Zyubin, A. M. Mebel, H. C. Chang, and S. H. Lin, Chemical Physics Letters **462**, 251 (2008).

23   I. B. Bersuker, in *The Jahn-Teller Effect* (Cambridge University Press, Cambridge, U.K., 2006).

24   M. Zlatar, M. Gruden-Pavlović, C.-W. Schläpfer, and C. Daul, Journal of Molecular Structure **954**, 86 (2010).

25   H. Ramanantoanina, M. Zlatar, P. Garcia-Fernandez, C. Daul, and M. Gruden-Pavlovic, Physical Chemistry Chemical Physics **15**, 1252 (2013).

26   L. Andjelković, M. Gruden-Pavlović, and M. Zlatar, Chemical Physics **460**, 64 (2015).

27   L. Andjelkovic, S. Stepanovic, F. Vlahovic, M. Zlatar, and M. Gruden, Physical Chemistry Chemical Physics **18**, 29122 (2016).

28   G. Kresse and J. Furthmüller, Phys. Rev. B **54**, 11169 (1996).

29   D. Alfè, Computer Physics Communications **180**, 2622 (2009).

30   C. Z. Wang and K. M. Ho, Phys. Rev. Lett. **71**, 1184 (1993).

31   M. Zlatar, C.-W. Schläpfer, and C. Daul, in *The Jahn-Teller Effect*, edited by H. Köppel, D. R. Yarkony and H. Barentzen (Springer Berlin Heidelberg, 2009), Vol. 97, p. 131.

32   M. Lax, The Journal of Chemical Physics **20**, 1752 (1952).

33   R. Kubo and Y. Toyozawa, Progress of Theoretical Physics **13**, 160 (1955).

34   J. J. Markham, Reviews of Modern Physics **31**, 956 (1959).

35   P. García-Fernández, I. B. Bersuker, J. A. Aramburu, M. T. Barriuso, and M. Moreno, Phys. Rev. B **71**, 184117 (2005).
36   N. B. Manson and J. P. Harrison, Diamond and Related Materials **14**, 1705 (2005).
37   G. Liaugaudas, G. Davies, K. Suhling, R. U. A. Khan, and D. J. F. Evans, Journal of Physics-Condensed Matter **24**, 435503 (2012).
38   K. Y. Wang, J. W. Steeds, Z. H. Li, and Y. M. Tian, Microscopy and Microanalysis **22**, 108 (2016).
39   A. R. Kun Huang, Proceedings of the Royal Society of London. Series A. Mathematical and Physical Sciences **204**, 406 (1950).
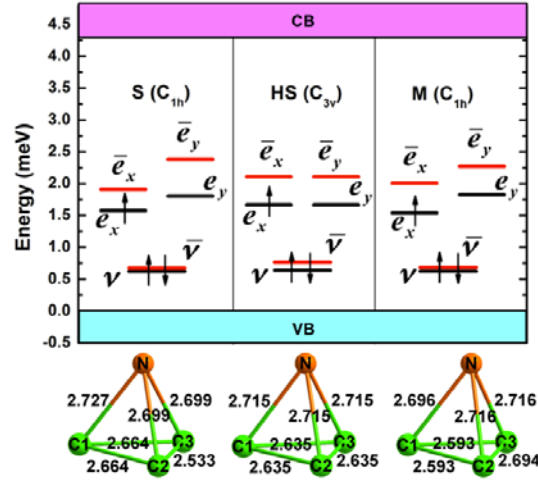
Figures and Tables:

FIG. 1. (Color online) Structures (lower panel) and relevant single-electron orbitals (upper panel) of the neutral NV^0 center in the ground state: the ^2E C_{3v} high symmetry state HS(middle), a distorted C_{1h} energy-minimum state M(right) and a saddle point state S(left). In the lower panel, only first neighbor C (green) and N (yellow) atoms to the vacant site are shown. In the C_{1h} state, one carbon (denoted as C1) is different from the two others (denoted as C2 and C3, and related to each other by reflection in the mirror plane {110}, passing through N, C1, and the vacancy site). In the C_{3v} state, these three C atoms are equivalent. The distances in unit Å between the first neighbor atoms are also shown. In the upper panel, the KS single-electron states between the valence band (VB) and conduction band (CB) are shown, with the top of VB as the reference energy. The symbols with a bar denote spin-down states, while the symbols without a bar correspond to spin-up states. The states ν and $\bar{\nu}$ have a_1 symmetry, all other states have e symmetry.
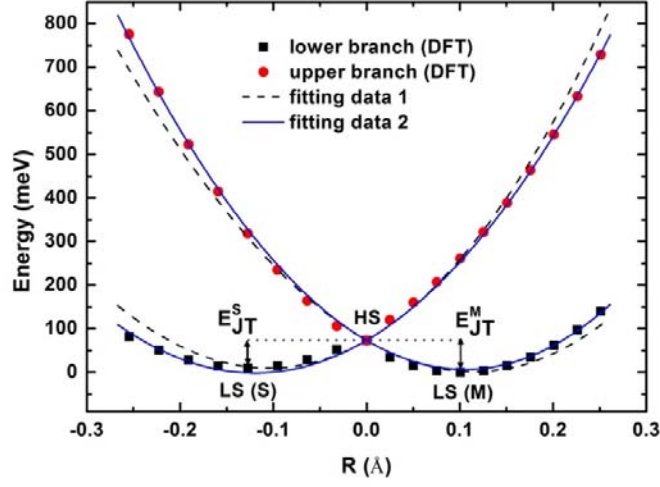
FIG. 2. (Color online) Adiabatic potential energy of the neutral NV^0 center along $\mathbf{R_{JT}}$ (positive) and $\mathbf{R_S}$ (negative) directions in the ground state via DFT calculations. All the points shown in the figure are *ab initio* energies which show the lower branch of ^2E state (black square points) and the upper branch of ^2E state (red circle points). The black dash and blue solid lines are quadratic fit of the *ab initio* energies based on Eq. (15) using the method 1 and 2, respectively as described in the text. The energy shown in the vertical axis is with respect to the energy of G_M.
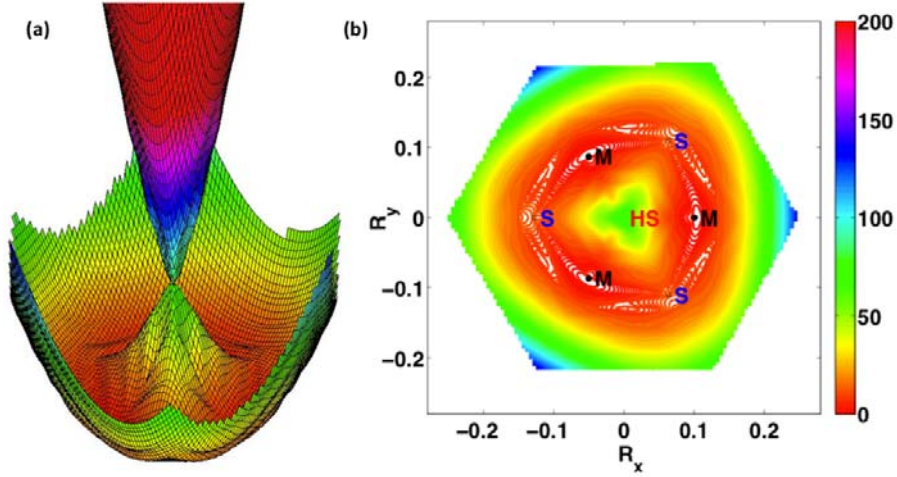

FIG. 3. (Color online) The adiabatic potential energy surface (APES) (a) and contour plot (b) of the lower sheet of ^2E state for the neutral NV center in diamond. The energy (in unit meV) shown in figure is with respect to the energy of G_M. R_x and R_y are in unit Å.
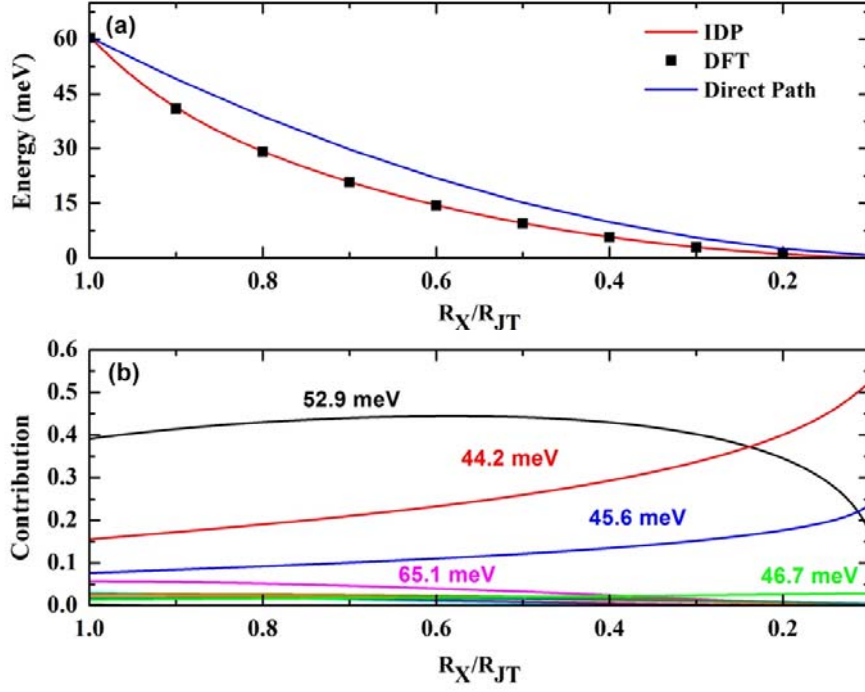
15

FIG. 4. (Color online) (a) Energy changes from the high symmetry G_{HS} (R_X/R_{JT}=1) to the low symmetry energy minimum G_M (R_X/R_{JT}=0) along the Direct Path and IDP respectively. The points shown in the (a) are the *ab initio* energies with the same geometries from the IDP. (b) The contributions (normalized to 1) to the JT distortion from the most important normal modes along the IDP from the high symmetry G_{HS} (R_X/R_{JT}=1) to the low symmetry energy minimum G_M (R_X/R_{JT}=0).
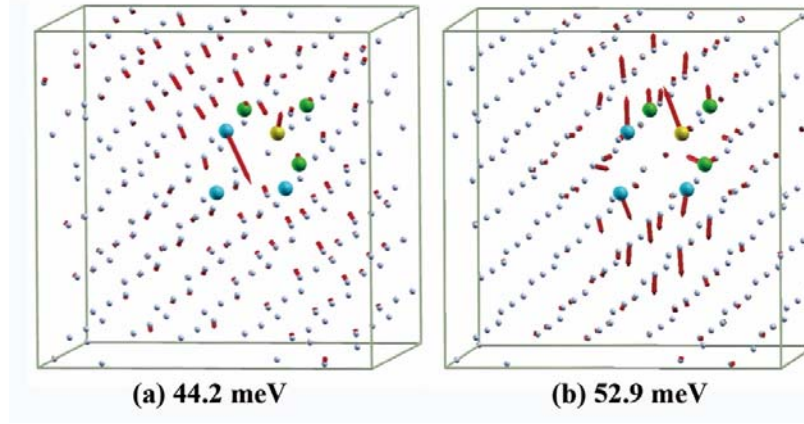

FIG. 5. (Color online) Two most important quasilocalized vibrational modes with energies of 44.2 meV (a) and 52.9 meV (b) in the energy minimum G_M of ground state of the neutral NV center, corresponding to the JT active vibrations. The red arrows show the eigenvector of atomic vibrations, the arrow length is proportional to the vibration amplitude of a given atom. Yellow spheres denote N atom, blue spheres denote the C atoms adjacent to the vacancy, green spheres denote the C atoms adjacent to the N atom. Small gray spheres are the other carbon atoms in the diamond lattice.
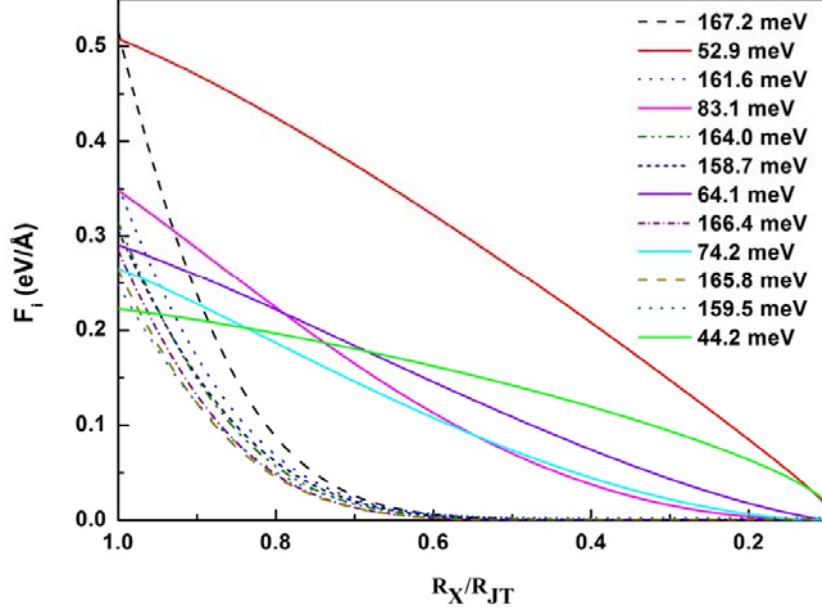
16

FIG. 6. (Color online) Forces from the modes that have larger contribution to the total force along IDP from the high symmetry G_{HS} ($R_x/R_{JT} = 1$) to the low symmetry energy minimum G_M.

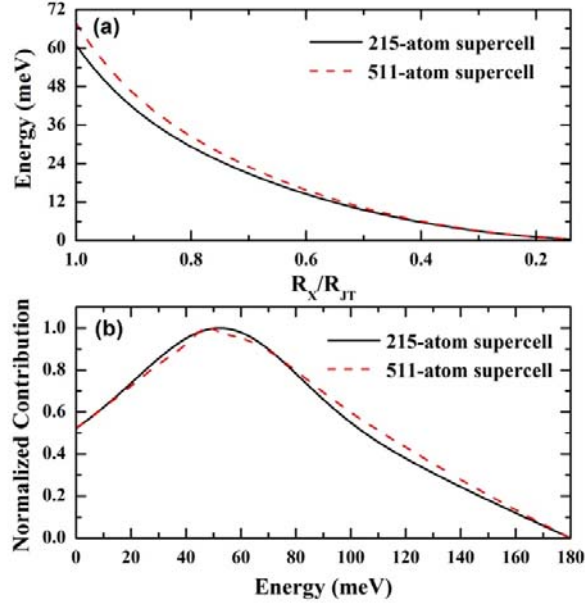FIG. 7. (Color online) (a) Energy changes from the high symmetry G_{HS} ($R_X/R_{JT}=1$) to the low symmetry energy minimum G_M ($R_X/R_{JT}=0$) along the IDP for 215-atom and 511-atom supercells respectively. (b) Normalized contribution of all the vibrational modes to the JT distortion ($R_X = R_{JT}$) in the 215-atom and 511-atom supercells. The maximum of the contribution of the vibration modes is normalized to 1 for comparing. The relaxation coordinate ($R_X = R_{JT}$) corresponding to the contributions is defined as $R_{JT;\alpha i} = R_{g(M);\alpha i} - R_{g(HS);\alpha i}$, where α

17

labels atoms, $i = \{x, y, z\}$, $R_{g(M);\alpha i}$ and $R_{g(HS);\alpha i}$ is the atomic position in the low symmetry minimum G_M and the high symmetry geometry G_{HS} in the ground state.
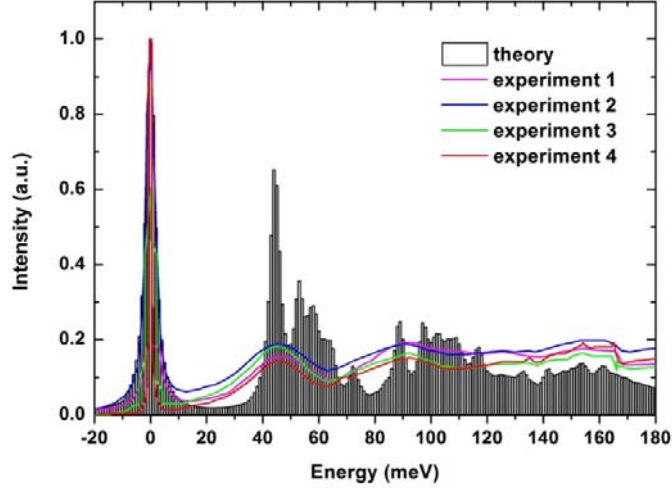

FIG. 8. (Color online) Normalized luminescence lineshapes for the neutral NV center in diamond. The energy shown in the horizontal axis is with respect to the energy of zero phonon line (E_{ZPL}= 2.156 eV). The calculated results (bar) are obtained using the method mentioned in the text. Three experimental results (1, 2, 3 and 4) are derived from reference 11, 36, 37, and 38.

TABLE I. Key parameters of the APES obtained from *ab initio* calculations

ρ_m (Å)	E_{JT}^m (meV)	ρ_s (Å)	E_{JT}^s (meV)	δ (meV)
0.101	73.2	0.127	63.2	10

TABLE II. Values of the vibronic coupling constants $V_{i\gamma}$ ($i = 1,2,3$; $\gamma = a, e$) of the NV^0 center obtained by fitting the *ab initio* data using the Eq. (20) and the two methods as explained in the text ($V_{i\gamma}$ *in* unit of eV/Å^i). The energy of the effective phonon mode is also shown.

Fitting method	V_{2a}	V_{3a}	V_{1e}	V_{2e}	$\hbar\omega$ (meV)
(I) $\varepsilon_{\pm}$	5.603	1.391	1.231	-0.496	62.5
(II) $(\varepsilon_+ \pm \varepsilon_-)/2$	5.612	0.446	1.137	-0.757	62.5

Table III. Calculated vibronic levels for the neutral NV center. The vibronic energies (I and II) are calculated with the JT parameters obtained from the different fitting methods (I and II) in the Table II. The original energies of vibronic levels shown in the Table are with respect to the energy of degenerate electronic ground state in the G_{HS}. The adjusted ones are with respect to the energy of the E vibronic ground state.

Symmetry	Energy I (meV)		Energy II (meV)	
	Original	Adjusted	Original	Adjusted
E	-29.2	0	-19.0	0
A_2	-5.4	23.8	2.4	21.4
A_1	1.6	30.8	19.5	38.5
E	32.3	61.5	42.8	61.8

E	44.4	73.6	58.2	77.2
A_1	71.8	100.0	82.8	101.8
E	78.4	107.6	90.1	109.1
A_2	85.5	114.7	103.6	122.6

TABLE IV. Analysis of the multimode JT effect in the ground state of NV^0 center: the JT radii (R_{JT}^k, (amu)$^{1/2}$ Å), the JT stationary energy (E_{JT}^k, meV), the contributions of the chosen normal modes to the distortion (c_r^k) and JT energy (c_e^k), and the inverse participation ratio (IPR_k).

Frequency, meV	R_{JT}^k, (amu)$^{1/2}$ Å	Contribution to R_{JT} (c_r^k, %)	E_{JT}^k, meV	Contribution to E_{JT} (c_e^k, %)	IPR_k
52.9	0.0395	39.1	15.9	26.1	0.014
44.2	0.0157	15.5	4.4	7.2	0.011
45.6	0.0077	7.6	2.3	3.8	0.007
65.1	0.0057	5.7	3.4	5.6	0.009
83.1	0.0031	3.1	3.0	4.9	0.010
74.2	0.0027	2.7	2.2	3.6	0.025
59.7	0.0026	2.6	1.3	2.1	0.007
64.2	0.0024	2.4	1.4	2.3	0.011
58.6	0.0018	1.8	0.9	1.5	0.016
64.8	0.0018	1.8	1.1	1.8	0.006
46.7	0.0014	1.4	0.4	0.7	0.007
72.3	0.0012	1.2	0.9	1.5	0.025
56.8	0.0011	1.1	0.5	0.8	0.013
76.3	0.0010	1.0	0.9	1.5	0.010
Total	0.0877	86.8	38.6	63.4	